IL NUOVO CIMENTO Vol. 25 C, N. 1 Gennaio-Febbraio 2002

Map projections and topography in atmospheric mesoscale modeling(*)

M. A. Núñez(**)

Departamento de Física, Universidad Autónoma Metropolitana - Iztapalapa
Apartado Postal 55-534, CP 09340 México, Distrito Federal, México

(ricevuto il 12 Maggio 2000; revisionato il 10 Maggio 2001; approvato il 7 Giugno 2001)

Summary. — Digital Elevation Models (DEMs) of the Earth surface are given by a data set $\{\lambda_k, \phi_k, h_k\}_{k=1}^K$, where h_k denotes the terrain height on a point (λ_k, ϕ_k) of an ellipsoidal Earth model $\mathcal{E}$. Map projections have been widely used in mesoscale modeling to get a DEM on a model domain $\mathcal{D}$ of a plane surface $\mathcal{P}$. The procedure consists in applying a map projection to each point (λ_k, ϕ_k) to get a point (X_k^p, Y_k^p) on $\mathcal{D}$ for which the correct terrain height Z_k^p is taken as h_k. This implies that $\mathcal{P}$ coincides with the tangent plane $\mathcal{T}$ to $\mathcal{E}$ at a point (λ_c, ϕ_c) which can be located at the centre of $\mathcal{D}$. In this work a method is proposed to get a DEM $\{X_k, Y_k, Z_k\}_{k=1}^K$ on $\mathcal{T}$ whose accuracy is similar to that of the original DEM $\{\lambda_k, \phi_k, h_k\}_{k=1}^K$; the method is extended to get a DEM on a spherical Earth model. The method is based on the transformation T that yields the point (X_k, Y_k) on $\mathcal{T}$ projected by a point $P_{\lambda\phi h}$ in the tridimesional space defined by the data λ_k, ϕ_k, h_k, T also yields the correct height Z_k of $P_{\lambda\phi h}$ with respect to the plane $\mathcal{T}$. By construction (X_k, Y_k) is the unique point in $\mathcal{T}$ for which the correct terrain height can be computed with the data λ_k, ϕ_k, h_k alone. It is shown that the points (X_k^p, Y_k^p) from map projections do not coincide with the corresponding one (X_k, Y_k), hence the correct height Z_k^p on each (X_k^p, Y_k^p) cannot be computed with the data λ_k, ϕ_k, h_k alone. The two immediate approximations $Z_k^p \sim Z_k$ and $Z_k^p \sim h_k$ are studied. The uncertainty $\Delta h_k = \pm 30$ m reported for a DEM is used to show that the estimations $Z_k^p \sim Z_k$ and $Z_k^p \sim h_k$ are valid on regions of 500×500 and 60×60 km^2, respectively. It is shown that if the point (X_k^p, Y_k^p) is near the boundary of a model domain of 1300×1300 km^2 the estimation $Z_k^p \sim h_k$ has an error of approximately 30 km, and for a domain of 3300×3300 km^2 the corresponding error may be 200 km. It is shown by means of analytic solutions of mesoscale meteorological equations that the innacuracy of the DEM $\{X_k^p, Y_k^p, h_k\}_{k=1}^K$ can yield a wrong wind field.

PACS 92.60 – Meteorology.
PACS 92.60.Wc – Weather analysis and prediction.
PACS 91.10.Ws – Reference systems.
PACS 91.10.Jf – Topography; geometric observations.

(*) The author of this paper has agreed to not receive the proofs for correction.
(**) E-mail: manp@xanum.uam.mx

1. – Introduction

Among the most important aspects of mesoscale meteorological models is their ability to resolve the influence of the Earth surface [1]. The standard way to describe the Earth surface consists in estimating the terrain height h_k on a point with longitude-latitude coordinates (λ_k, ϕ_k) on an ellipsoidal Earth model $\mathcal{E}$, the complete data set $\{\lambda_k, \phi_k, h_k\}_{k=1}^K$ is referred to as a Digital Elevation Model (DEM) [2]. DEMs play a basic role in the numerical solution of mesoscale model equations because they determine i) the minimun horizontal grid spacing to describe accurately the topography in a model domain and ii) the σ-type vertical coordinates, which have shown to be an efficient way to incorporate topographic irregularities into the model equations [1, 3-5]. Most present day mesoscale models use conformal map projections to represent the Earth surface on a plane surface and to generate a DEM on a Cartesian regularly-spaced computational grid [1, 6-11]. The procedure described in ref. [11] is as follows. A Cartesian coordinate system X^pY^p is chosen on the so-called projection plane $\mathcal{P}$ and the origin can be located at the center of the model domain $\mathcal{D}$ in $\mathcal{P}$, if r is the distance from the center of the Earth and a denotes the mean radius of the Earth the vertical coordinate Z^p on $\mathcal{P}$ is taken as $Z^p = r - a$. To obtain a DEM on $\mathcal{P}$ from a given DEM $\{\lambda_k, \phi_k, h_k\}_{k=1}^K$ a conformal map projection is applied to the data λ_k, ϕ_k to get a point (X_k^p, Y_k^p) on $\mathcal{D}$ and it is assumed that the correct terrain height Z_k^p on (X_k^p, Y_k^p) is the correspoding datum h_k because the distortion of the spherical Earth shape is small with map projections [4, 6-11]. Thus a DEM $\{X_k^p, Y_k^p, h_k\}$ is obtained on $\mathcal{P}$. Since the points (X_k^p, Y_k^p) do not coincide with those (X_m^r, Y_m^r) of a regularly-spaced computational grid on $\mathcal{D}$ the elevation data h_k are interpolated to get an average height $\langle Z_m^r \rangle$ on each (X_m^r, Y_m^r) by means of a weighted sum $\langle Z_m^a \rangle = \sum_k W_{mk} h_k$ (see, *e.g.*, [8, 9]). Additionally some models include metric factors in the horizontal derivatives of model equations to consider map projections [6, 11]. There are two basic questions about this approach to get DEMs on $\mathcal{P}$ that, for the knowledge of the author, have not been studied in the mesoscale literature: i) the region $\mathcal{R}$ in $\mathcal{P}$ where is valid to take Z_k^p as h_k and ii) the error of such an approach. The main aim of this article is i) to propose a method that yields a DEM on $\mathcal{P}$ whose accuracy is similar to that of the original DEM $\{\lambda_k, \phi_k, h_k\}$ and to apply this approach to generate a DEM on a spherical Earth model, and ii) to carry out an uncertainty analysis of the DEMs $\{X_k^p, Y_k^p, h_k\}$ obtained with map projections.

In subsect. **2**˙1 we introduce the primary Cartesian system xyz associated to an ellipsoidal Earth model $\mathcal{E}$ and the geodetic coordinates λ, ϕ, h of an arbitrary point P in the tridimensional space. In subsect. **2**˙2 we consider the tangent plane $\mathcal{T}$ to $\mathcal{E}$ at a point $P_c = (\lambda_c, \phi_c)$ and a Cartesian coordinate system XYZ on $\mathcal{T}$ with is origin at P_c. The transformation T that yields the coordinates X, Y, Z of a point P with coordinates λ, ϕ, h, is given. It is shown that the application of T to the data of a DEM $\{\lambda_k, \phi_k, h_k\}$ on $\mathcal{E}$ generates a DEM $\{X_k, Y_k, Z_k\}$ on $\mathcal{T}$ whose accuracy is similar to that of the DEM $\{\lambda_k, \phi_k, h_k\}$. In subsect. **2**˙3 we propose a spherical Earth model $\mathcal{S}$ and a spherical coordinate system Λ, Φ, H to generate a reliable DEM on $\mathcal{S}$.

In the theory of map projections the description of the projection plane $\mathcal{P}$ is ambiguous because it may be a flat sheet of paper or the tangent plane $\mathcal{T}$ to the Earth model $\mathcal{E}$ [12, 13]. In sect. **3** we adopt P_c as the center of a model domain $\mathcal{D}$ in $\mathcal{P}$ and it is shown that $\mathcal{P}$ coincides with $\mathcal{T}$ when the geodetic height h_c of the irregular Earth surface on P_c is taken as the exact terrain height Z_c on P_c. This identification of $\mathcal{P}$ and the transformation T allows us to analyze the DEMs $\{X_k^p, Y_k^p, h_k\}$ from map projections. First, it is shown that the DEM $\{X_k, Y_k, Z_k\}$ obtained with the transformation T has the

unique points (X_k, Y_k) on $\mathcal{T}$ for which the correct terrain height (Z_k) can be computed, we then show that the points (X_k^p, Y_k^p) from map projections do not coincide with the corresponding one (X_k, Y_k), a result that poses the problem of estimating the correct height Z_k^p on (X_k^p, Y_k^p). The two immediate approximations $Z_k^p \sim Z_k$ and $Z_k^p \sim h_k$ are studied in subsects. **3**˙1 and **3**˙2. The uncertainty reported for data of the DEM called GTOPO30 [14] and the DEM $\{X_k, Y_k, Z_k\}$ from T are used to estimate the region $\mathcal{R}$ of $\mathcal{T}$ where each approximation is valid. The results show that $\mathcal{R}$ can be significantly smaller than the computational model region $\mathcal{D}$ used in some mesoscale studies [15-17]. In sect. **4** we compare model equations provided by the correct representation of topography with those obtained via map projections. Analytic and stationary solutions of these equations show that the innacuracy of a map-projection topography can generate a wrong wind field. Section **5** contains some concluding remarks.

2. – Geodetic, Cartesian and spherical coordinate systems

2˙1. *Ellipsoidal Earth model $\mathcal{E}$, coordinates x, y, z and λ, ϕ, h, and the DEM $\{\lambda_k, \phi_k, h_k\}$.* – The standard mathematical model of the Earth is an ellipsoid of revolution (which we denote by $\mathcal{E}$) whose axis of revolution is taken as the z-axis of a primary Cartesian coordinate system xyz with its origin at the center of $\mathcal{E}$. Thus $\mathcal{E}$ is described by the equation $(x^2 + y^2)/a^2 + z^2/b^2 = 1$, where a and b are the major and minor axes, respectively. The location of each point on $\mathcal{E}$ is defined by the geodetic latitude ϕ and longitude λ which yield the Cartesian coordinates of the point,

$$x = f_x(\lambda, \phi) \equiv N(\phi) \cos\phi \cos\lambda\,, \tag{2.1a}$$

$$y = f_y(\lambda, \phi) \equiv N(\phi) \cos\phi \sin\lambda\,, \tag{2.1b}$$

$$z = f_z(\lambda, \phi) \equiv N(\phi)(1 - \epsilon^2) \sin\phi\,, \tag{2.1c}$$

with $N(\phi) = a(1 - \epsilon^2 \sin^2\phi)^{-1/2}$, $\epsilon^2 = 1 - (a/b)^2$, $\lambda \in (-\pi, \pi]$ and $\phi \in [-\pi/2, \pi/2]$ [13]. If $\hat{\mathbf{x}}$, $\hat{\mathbf{y}}$, $\hat{\mathbf{z}}$ denote the unitary vectors along the positive x, y, z axes, respectively, $\mathcal{E}$ has the vectorial equation

$$\tilde{\mathbf{r}}_{\mathcal{E}}(\lambda, \phi) = \hat{\mathbf{x}} f_x(\lambda, \phi) + \hat{\mathbf{y}} f_y(\lambda, \phi) + \hat{\mathbf{z}} f_z(\lambda, \phi). \tag{2.2}$$

The latitude ϕ is the angle between the equatorial xy plane and the vector $\hat{\mathbf{N}}(\lambda, \phi)$ normal to $\mathcal{E}$ at (λ, ϕ) [12],

$$\hat{\mathbf{N}}(\lambda, \phi) = (\hat{\mathbf{x}} \cos\lambda + \hat{\mathbf{y}} \sin\lambda) \cos\phi + \hat{\mathbf{z}} \sin\phi. \tag{2.3}$$

Throughout the paper we take ϕ positive on the North hemisphere and the reference meridian to measure λ is on the xz plane and intersects the positive x-axis, λ is positive Eastward (negative Westward), see fig. 1.

Every point P in the tridimensional space projects on $\mathcal{E}$ a unique point (λ_P, ϕ_P) and if h_P denotes the distance from (λ_P, ϕ_P) to P with $h_P > 0$ ($h_P < 0$) for P out of (into) $\mathcal{E}$, then P can be represented with the Cartesian coordinates (x_P, y_P, z_P) or the geodetic ones (λ_P, ϕ_P, h_P). Thus if $\vec{\mathbf{r}}_P$ denotes the vector from the origin to P we have $\vec{\mathbf{r}}_P = \hat{\mathbf{x}} x_P + \hat{\mathbf{y}} y_P + \hat{\mathbf{z}} z_P = \vec{\mathbf{r}}_{\mathcal{E}}(\lambda_P, \phi_P) + h_P \hat{\mathbf{N}}(\lambda_P, \phi_P)$ (see fig. 2). This together with

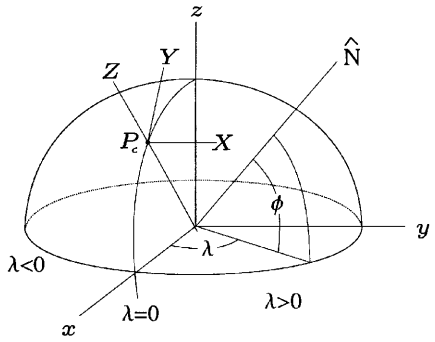

Fig. 1. – Primary Cartesian coordinate system xyz with its origin at the center of $\mathcal{E}$, Cartesian system XYZ and geodetic coordinates λ, ϕ.

(2.1)-(2.3) leads to the transformation equations

$$x_P = f_x(\lambda_P, \phi_P) + h_P \cos\phi_P \cos\lambda_P \,, \tag{2.4a}$$

$$y_P = f_y(\lambda_P, \phi_P) + h_P \cos\phi_P \sin\lambda_P \,, \tag{2.4b}$$

$$z_P = f_z(\lambda_P, \phi_P) + h_P \sin\phi_P \,, \tag{2.4c}$$

which will be denoted by

$$(x_P, y_P, z_P) = E(\lambda_P, \phi_P, h_P). \tag{2.5}$$

The inverse transformation $E^{-1}(x_P, y_P, z_P) = (\lambda_P, \phi_P, h_P)$ can be computed as follows.

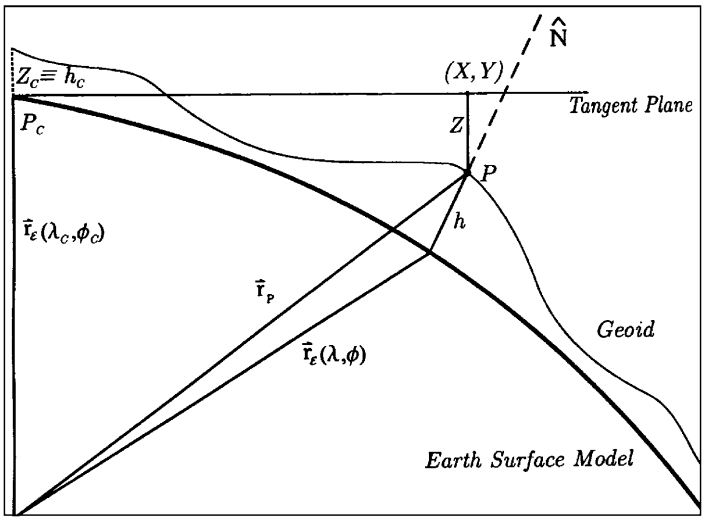

Fig. 2. – Sketch of the plane $\mathcal{T}$ tangent to $\mathcal{E}$ at $P_c = (\lambda_c, \phi_c)$ and the Geoid. The point P on the geoid has Cartesian coordinates x, y, z and geodetic ones λ, ϕ, h with respect to the system xyz, and X, Y, Z are their coordinates with respect to the system XYZ.

Using (2.1) and (2.4) we get

$$\lambda_P = \tan^{-1}(y_P/x_P). \tag{2.6}$$

In general ϕ_P and h_P must be computed numerically, we found that the numerical calculation is easier with the parameterization of $\mathcal{E}$ given by

$$x = g_x(\lambda,\phi') \equiv a\cos\phi'\cos\lambda\,, \qquad z = g_z(\lambda,\phi') \equiv b\sin\phi'\,, \tag{2.7a}$$

$$y = g_y(\lambda,\phi') \equiv a\cos\phi'\sin\lambda\,; \tag{2.7b}$$

from (2.1) and (2.7) there follows the relationship $\tan\phi' = (1-\epsilon^2)^{1/2}\tan\phi$. Let $(\lambda_P, \phi'_P, h_P)$ be the new representation of P. Since the point (λ_P, ϕ'_P) is the unique one that minimizes the Euclidean distance between $P = (x_P, y_P, z_P)$ and $\mathcal{E}$ and the minimun distance is $|h_P|$, the distance function

$$d(\lambda,\phi') = \{[g_x(\lambda,\phi') - x_P]^2 + [g_y(\lambda,\phi') - y_P]^2 + [g_z(\lambda,\phi') - z_P]^2\}^{1/2} \tag{2.8}$$

satisfies the equation

$$\frac{\partial d(\lambda_P,\phi'_P)}{\partial\phi'} = 0\,, \tag{2.9}$$

whose numerical solution yields ϕ'_P, hence we get

$$\phi_P = \tan^{-1}[(1-\epsilon^2)^{-1/2}\tan\phi'_P], \qquad |h_P| = d(\lambda_P,\phi'_P). \tag{2.10}$$

Since ϵ^2 is small we set $\epsilon = 0$ in (2.9) to get the accurate approximation $[\phi'_P]^{(0)} = \tan^{-1}[z_P/(x_P\cos\lambda_P + y_P\sin\lambda_P)]$, which can be improved with the Newton-Raphson method to get ϕ'_P with the desired accuracy.

Remark 1. In the literature of geodesy the irregular Earth surface is called Geoid [2], see fig. 2. The geodetic position of a point P on the Geoid is defined by the coordinates λ_P, ϕ_P, h_P, where h_P is, in principle, given by a function $\mathrm{top}(\lambda_P,\phi_P)$ ([2], p. 56). In practice the function $\mathrm{top}(\lambda_P,\phi_P)$ is known on a finite set $\{\lambda_k,\phi_k\}_{k=1}^K$ of $\mathcal{E}$, in this case we set $h_k \equiv \mathrm{top}(\lambda_k,\phi_k)$ and the complete DEM of the Geoid is denoted by $\{\lambda_k,\phi_k,h_k\}$. When the accuracy is not critical the terrain elevation above or below the mean sea level can or has been used as an estimation of the geodetic height h, as occurs with the data of the DEM called GTOPO30 in which the elevation data are referenced to the mean sea level [14].

2˙2. *Tangent plane, coordinates X, Y, Z and the DEM* $\{X_k, Y_k, Z_k\}$. – Let $\mathcal{T}$ denote the plane tangent to $\mathcal{E}$ at the point $P_\mathrm{c} = (\lambda_\mathrm{c},\phi_\mathrm{c})$ on the zero meridian $\lambda_\mathrm{c} = 0$. The following Cartesian coordinate XYZ system is adopted on $\mathcal{T}$: the origin $X = Y = Z = 0$ is at P_c, the X-axis is tangent to the parallel circle at P_c and positive Eastward, the Y-axis is tangent to the zero meridian and positive Northward, the positive Z-axis is taken out of $\mathcal{E}$, see fig. 1. If $\hat{\mathbf{X}}$, $\hat{\mathbf{Y}}$, $\hat{\mathbf{Z}}$ denote the unitary vectors along the positive X, Y and Z axes, respectively, they are given by

$$\hat{\mathbf{X}} = \hat{\mathbf{y}}, \quad \hat{\mathbf{Y}} = -\hat{\mathbf{x}}\sin\phi_\mathrm{c} + \hat{\mathbf{z}}\cos\phi_\mathrm{c}, \quad \hat{\mathbf{Z}} = \hat{\mathbf{x}}\cos\phi_\mathrm{c} + \hat{\mathbf{z}}\sin\phi_\mathrm{c}, \tag{2.11}$$

where $\hat{\mathbf{Z}} = \hat{\mathbf{N}}(\lambda_c, \phi_c)$. Let P be a point with coordinates λ_P, ϕ_P, h_P and let X_P, Y_P, Z_P be their coordinates with respect to the XYZ system. If $\vec{\mathbf{r}}_P$ is the vector from the origin $x = y = z = 0$ to P the equation (see fig. 2)

$$\vec{\mathbf{r}}_P = \hat{\mathbf{x}}x_P + \hat{\mathbf{y}}y_P + \hat{\mathbf{z}}z_P = \vec{\mathbf{r}}_{\mathcal{E}}(\lambda_c, \phi_c) + \hat{\mathbf{X}}X_P + \hat{\mathbf{Y}}Y_P + \hat{\mathbf{Z}}Z_P \tag{2.12}$$

holds with $(x_P, y_P, z_P) = E(\lambda_P, \phi_P, h_P)$ (eqs. (2.4*a-c*)). This together with (2.11) yields the transformation equations

$$X_P = T_X(\lambda_P, \phi_P, h_P) = f_y(\lambda_P, \phi_P) + h_P \cos\phi_P \sin\lambda_P\,, \tag{2.13a}$$

$$Y_P = T_Y(\lambda_P, \phi_P, h_P) = C_2 \cos\phi_c - C_1 \sin\phi_c\,, \tag{2.13b}$$

$$Z_P = T_Z(\lambda_P, \phi_P, h_P) = C_2 \sin\phi_c + C_1 \cos\phi_c\,, \tag{2.13c}$$

where

$$C_1 = f_x(\lambda_P, \phi_P) - f_x(\lambda_c, \phi_c) + h_P \cos\phi_P \cos\lambda_P\,, \tag{2.13d}$$

$$C_2 = f_z(\lambda_P, \phi_P) - f_z(\lambda_c, \phi_c) + h_P \sin\phi_P\,. \tag{2.13e}$$

These equations will be denoted by

$$(X_P, Y_P, Z_P) = T(\lambda_P, \phi_P, h_P). \tag{2.14}$$

The inverse transformation $(\lambda_P, \phi_P, h_P) = T^{-1}(X_P, Y_P, Z_P)$ is obtained with (2.11)-(2.13) to compute the coordinates x_P, y_P, z_P, which in turn yield $E^{-1}(x_P, y_P, z_P) = (\lambda_P, \phi_P, h_P)$ (eqs. (2.6)-(2.10)).

If a point on the Geoid has coordinates λ_k, ϕ_k, h_k their coordinates with respect to the system XYZ are $(X_k, Y_k, Z_k) = T(\lambda_k, \phi_k, h_k)$ and if the uncertainty $\Delta\lambda_k$, $\Delta\phi_k$, Δh_k is known the uncertainty ΔX_k can be estimated with the formula

$$\Delta X_k = \Delta\lambda_k \partial T_X/\partial\lambda + \Delta\phi_k \partial T_X/\partial\phi + \Delta h_k \partial T_X/\partial h \tag{2.15}$$

and similar expressions are used for ΔY_k and ΔZ_k. For example, data from GTOPO30 for México and E.U.A. are reported with $\Delta\lambda_k = \Delta\phi_k = 0$ [14], in this case we have

$$|\Delta X_k| \le |\Delta h_k|, \quad |\Delta Y_k| \le 2|\Delta h_k|, \quad |\Delta Z_k| \le 2|\Delta h_k|. \tag{2.16}$$

Thus we get a DEM $\{X_k, Y_k, Z_k\}$ on $\mathcal{T}$ whose accuracy is similar to that of the original DEM $\{\lambda_k, \phi_k, h_k\}$ on $\mathcal{E}$.

2˙3. *Tangent sphere, coordinates Λ, Φ, H and the DEM $\{\Lambda_k, \Phi_k, H_k\}$.* – The mathematical modeling of some synoptic and mesoscale flows should consider the curvature of the Earth, this can be done with a suitable spherical Earth model denoted by $\mathcal{S}$. The sphere considered in this work is tangent to $\mathcal{E}$ at a point $P_c = (\lambda_c, \phi_c)$ on the zero meridian $\lambda_c = 0$. The radius R_s of $\mathcal{S}$ is not unique but following Driencourt we may propose

$$R_s = a(1-\epsilon^2)^{1/2}(1-\epsilon^2\sin^2\phi_c)^{-1} \tag{2.17}$$

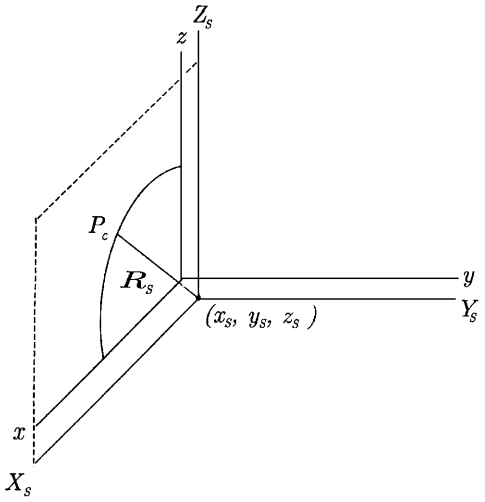

Fig. 3. – Primary system xyz and system $X_sY_sZ_s$ with its origin at the center (x_s, y_s, z_s) of the tangent sphere $\mathcal{S}$.

because it yields a certain minimun distortion from $\mathcal{E}$ to $\mathcal{S}$ ([13], p. 24).

With a given R_s and the vector $\hat{\mathbf{N}}(\lambda_c, \phi_c)$ normal to $\mathcal{E}$ at P_c (eq. (2.3)) we get the coordinates of the center of $\mathcal{S}$ with respect to the primary system xyz,

$$x_s = [N(\phi_c) - R_s]\cos\phi_c, \quad y_s = 0, \quad z_s = [(1-\epsilon^2)N(\phi_c) - R_s]\sin\phi_c. \tag{2.18}$$

We now adopt the Cartesian coordinate system $X_sY_sZ_s$ for which the origin $X_s = Y_s = Z_s = 0$ is at the center of $\mathcal{S}$, the X_sZ_s-plane coincides with that of the system xyz and the positive X_s, Y_s, Z_s axes have the orientation of the corresponding axes of the xyz system, see fig. 3. Thus the transformation equations between the coordinate systems $X_sY_sZ_s$ and xyz are

$$X_s = x - x_s, \quad Y_s = y, \quad Z_s = z - z_s. \tag{2.19}$$

If a point P has coordinates X_{sP}, Y_{sP}, Z_{sP} their spherical coordinates Λ_P, Φ_P, H_P are defined by the equations

$$X_{sP} = (R_s + H_P)\cos\Phi_P\cos\Lambda_P\,, \tag{2.20a}$$

$$Y_{sP} = (R_s + H_P)\cos\Phi_P\sin\Lambda_P\,, \tag{2.20b}$$

$$Z_{sP} = (R_s + H_P)\sin\Phi_P\,, \tag{2.20c}$$

with $\Lambda_P \in (-\pi, \pi]$, $\Phi_P \in [-\pi/2, \pi/2]$, $H_P \in [-R_s, \infty)$; positive values of Λ_P and Φ_P are taken Eastward and Northward, respectively, and H_P is positive for P out of $\mathcal{S}$. Since the latitude ϕ_c of P_c is the angle between the vector $\hat{\mathbf{N}}(\lambda_c, \phi_c)$ and the x-axis and this axis is parallel to the X_s-axis, P_c is the unique point for which the coordinates λ_P, ϕ_P, h_P coincide with Λ_P, Φ_P, H_P, respectively.

The transformation equations from the coordinates λ_P, ϕ_P, h_P to Λ_P, Φ_P, H_P for a point P are represented by

$$(\Lambda_P, \Phi_P, H_P) = S(\lambda_P, \phi_P, h_P) \tag{2.21}$$

and are obtained as follows. First we apply $E(\lambda_P, \phi_P, h_P) = (x_P, y_P, z_P)$ (eqs. (2.4*a-c*)), then we compute $X_{sP} = x_P - x_{\mathcal{S}}$, $Y_{sP} = y_P$, $Z_{sP} = z_P - z_{\mathcal{S}}$ and using (2.20*a-c*) we get

$$\Phi_P = \tan^{-1}[Z_{sP}/(X_{sP}^2 + Y_{sP}^2)^{1/2}], \Lambda_P = \tan^{-1}[Y_{sP}/X_{sP}], \tag{2.22a}$$

$$H_P = (X_{sP}^2 + Y_{sP}^2 + Z_{sP}^2)^{1/2} - R_s. \tag{2.22b}$$

The inverse transformation $S^{-1}(\Lambda_P, \Phi_P, H_P) = (\lambda_P, \phi_P, h_P)$ is obtained from (2.20*a-c*), (2.19) and the application of E^{-1} (eqs. (2.6)-(2.10)).

The application of S to the data λ_k, ϕ_k, h_k of a DEM $\{\lambda_k, \phi_k, h_k\}$ on $\mathcal{E}$ generates a DEM $\{\Lambda_k, \Phi_k, H_k\}$ on $\mathcal{S}$ whose uncertainty can be estimated with equations similar to (2.16).

3. – Analysis of map projections

The main aim of map projections is to transfer points on an ellipsoidal Earth model $\mathcal{E}$ to corresponding points on "a flat sheet of paper" which is usually referred to as the projection plane and we denote it by $\mathcal{P}$. Let (λ, ϕ) be a point on $\mathcal{E}$, the map projections are defined by a pair of equations

$$X^p = P_X(\lambda, \phi), \quad Y^p = P_Y(\lambda, \phi), \tag{3.1}$$

where X^p and Y^p are the coordinates of the point corresponding to (λ, ϕ) with respect to a rectangular Cartesian coordinate system defined on $\mathcal{P}$. The common rectangular system adopted has positive Y^p- and X^p-axes pointing to the North and East, respectively, and if the origin of the X^pY^p system has coordinates (λ_0, ϕ_0) eq. (3.1) becomes

$$P_X(\lambda_0, \phi_0) = 0, \quad P_Y(\lambda_0, \phi_0) = 0. \tag{3.2}$$

The description of $\mathcal{P}$ is ambiguous because as a rule (conformal) map projections cannot be represented geometrically ([13], p. 72), except the stereographic projection of a sphere, and the map-making process may use a fictitious geometric surface which is developed by flattening into a plane surface ($\mathcal{P}$). To analyze the use of map projections to get a DEM it is necessary a precise definition of $\mathcal{P}$ with respect to the primary coordinate system used to define the original DEM $\{\lambda_k, \phi_k, h_k\}$. Without loss of generality we assume that $\{\lambda_k, \phi_k, h_k\}$ is referenced to the xyz system of subsect. **2**˙1, the problem is then to define mathematically $\mathcal{P}$ in such a primary system. As is known this can be done with i) the coordinates of one point in $\mathcal{P}$ and ii) any vector normal to $\mathcal{P}$. Consider a map projection for which the point on the zero meridian $P_c = (\lambda_c = 0, \phi_c)$ corresponds to the center of the model domain $\mathcal{D}$ and is located at the origin of the X^pY^p system on $\mathcal{P}$,

$$P_X(0, \phi_c) = P_Y(0, \phi_c) = 0, \tag{3.3}$$

thus we have a point P_c on $\mathcal{P}$ whose coordinates x, y, z are known (eqs. (2.1*a-c*)). To give one vector normal to $\mathcal{P}$ and to clarify what is the correct terrain height on the points

(X^p, Y^p) from map projections it is convenient to consider the generally accepted notion of terrain height which we adopt as *Definition 1*: The terrain height on a point P of a surface S is the distance between P and the Geoid along a (predetermined) vector $\hat{\mathbf{n}}_P$ normal to S at P whose orientation determines the sign of the height. This is congruent with the definition of geodetic height h_c on P_c for which the normal vector is $\hat{\mathbf{N}}(\lambda_c, \phi_c)$ (see Remark 1). In the case of the projection plane $\mathcal{P}$ there is only one normal vector $\hat{\mathbf{n}}_P$ (module a scalar factor) which can be determined as follows. If we assume that the *exact* terrain height Z_c on P_c (which is seen as an element of $\mathcal{P}$) is the height h_c of the Geoid on P_c, then the vector normal to $\mathcal{P}$ at P_c is $\hat{\mathbf{N}}(\lambda_c, \phi_c)$ (fig. 2). Thus, P_c and $\hat{\mathbf{N}}(\lambda_c, \phi_c)$ define uniquely $\mathcal{P}$ with respect to the primary system xyz, but this is one way to define the plane $\mathcal{T}$ tangent to $\mathcal{E}$ at P_c (subsect. **2**˙2), therefore $\mathcal{P} = \mathcal{T}$.
Remark 2: The definition $Z_c \equiv h_c$ is consistent with the approximation $Z_k \sim h_k$ used in mesoscale modeling to define DEMs via map projections (sect. **1**) but it is clear that for another point (X_k^p, Y_k^p) on $\mathcal{P}$ the correct height Z_k^p cannot be the corresponding geodetic height h_k because of the curvature of $\mathcal{E}$ (fig. 2).

To end the identification of $\mathcal{P}$ we consider that the unit of length in the axes of the systems xyz and X^pY^p is the same, thus the axes X^p and Y^p coincide with those of the XYZ system defined on $\mathcal{T}$ (subsect. **2**˙2). In particular every point (X^p, Y^p) obtained from a point (λ, ϕ, h) on the Geoid with a map projection that satisfies (3.3), has coordinates

$$X = X^p\,, \qquad Y = Y^p\,, \qquad Z = 0\,,$$

with respect to the system XYZ and the terrain height on (X^p, Y^p) is exactly the vertical coordinate Z^p of (λ, ϕ, h) in the system XYZ (fig. 2).

Let us now consider the definition and estimation of a DEM on $\mathcal{T}$ when we have a DEM $\{\lambda_k, \phi_k, h_k\}$ on $\mathcal{E}$. Suppose that $\{\lambda_k, \phi_k, h_k\}$ has *null* uncertainty, let (X_k^p, Y_k^p) denote the point obtained from (λ_k, ϕ_k) with a map projection (3.1) that satisfies (3.3) and let Z_k^p denote the *true* terrain elevation on (X_k^p, Y_k^p) with respect to the XYZ system. The common practice for estimating Z_k^p is to take

$$Z_k^p \sim h_k\,, \tag{3.4}$$

because map projections generate a minimun distortion of the Earth surface [4,6-11]. To analyse this approximation in mesoscale modeling we have to bear in mind the following features of the transformation T (2.14). First, T has no relationship with conformal map projections, it gives the coordinates X_P, Y_P, Z_P of a point P in the system XYZ when it has coordinates λ_P, ϕ_P, h_P with respect to the primary system xyz. In particular every point (λ_k, ϕ_k, h_k) has a unique representation with respect to the system XYZ given by $(X_k, Y_k, Z_k) = T(\lambda_k, \phi_k, h_k)$. The geometric interpretation is easy: fig. 2 shows that the point (λ_k, ϕ_k, h_k) on the Geoid projects a unique point (X_k, Y_k) on $\mathcal{T}$ that is Z_k units of length away from (λ_k, ϕ_k, h_k), along the vector $\hat{\mathbf{Z}}$ normal to $\mathcal{T}$, hence Z_k is also the exact terrain height on (X_k, Y_k) (Definition 1). Thus, T yields the *unique* points (X_k, Y_k) on $\mathcal{T}$ for which we can compute the correct terrain height Z_k by using the data λ_k, ϕ_k, h_k *alone*. It is clear that the transformation T is not conformal but this "deficiency" is apparent because T considers the datum h_k to yield the correct height Z_k on (X_k, Y_k) whereas *no* conformal projection considers such a piece of information. Thus, it is expected that the point (X_k, Y_k) does not coincide with that (X_k^p, Y_k^p) from a map projection, except on some few places. This expectation is confirmed below and

poses the problem of estimating the correct height Z_k^p on each point (X_k^p, Y_k^p). The two immediate approximations $Z_k^p \sim Z_k$ and $Z_k^p \sim h_k$ are studied below.

By simplicity we consider the WGS84 ellipsoid $\mathcal{E}$ [2] with $a = 6378.1$ km, $\epsilon^2 = 6.7 \times 10^{-3}$ (which is approximated by $\epsilon^2 = 0$ to simplify projection formulae), and a zero terrain elevation on $\mathcal{E}$,

$$h = \text{top}(\lambda, \phi) \equiv 0.$$

According to our assumptions, $\mathcal{T}$ is tangent to $\mathcal{E}$ at $P_c = (\lambda_c, \phi_c)$ which is the origin of the XYZ system of subsect. **2**˙2 and the center of a rectangular domain $\mathcal{D}$ denoted by

$$[-X_{\max}, X_{\max}] \times [-Y_{\max}, Y_{\max}]. \tag{3.5}$$

We have $\lambda_c = 0$ and the value $\phi_c = 24^\circ$ was chosen. There are three domains $\mathcal{D}$ of interest in $\mathcal{T}$. An operational application of the Mesoscale Model 5 (MM5) [7, 8] in Mexico [15] uses a Lambert projection to define a model domain with its center at $\phi = 24^\circ$ and 101° of longitude from the Greenwich meridian, the horizontal mesh consists of 75×75 points separated by 45 km, this yields the domain $\mathcal{D}_a$ given by (3.5) with

$$X_{\max} = Y_{\max} = 1665 \quad \text{km}.$$

A recent study of mesoscale flows in Mexico [16] employed the Regional Atmospheric Modeling System (RAMS) with a Stereographic projection [6] on a domain of 1764×1764 km^2, this defines the domain $\mathcal{D}_b$ given by (3.5) with

$$X_{\max} = Y_{\max} = 882 \quad \text{km}.$$

A mercator projection was used in [17] to define a domain of approximately 1600×1300 km^2; we consider the domain $\mathcal{D}_c$ given by (3.5) with

$$X_{\max} = Y_{\max} = 650 \quad \text{km}.$$

The projections considered below are the Oblique Stereographic Projection (OSP), the Universal Transverse Mercator Projection (UTM), the Lambert Projection with one standard parallel at ϕ_c (LP1) and two standard parallels at $\phi_1 = 14^\circ$ and $\phi_2 = 34^\circ$ (LP2); the formulae from [12, 13] were modified to satisfy (3.3) and are given in the appendix.

3˙1. *Approximation* $Z_k^p \sim Z_k$. – Figure 4 shows some points (X_k, Y_k) and (X_k^p, Y_k^p) on the domain $\mathcal{D}_a$ of $\mathcal{T}$, we see that the point (X_k^p, Y_k^p) from one projection is near to that of another projection and each set $\{X_k^p, Y_k^p\}$ is almost rectangular in a region with its center at $X = 0$, $Y = 0$ as expected by the use of conformal projections. The apparent closeness between (X_k, Y_k) and the point (X_k^p, Y_k^p) from a map projection is reflected by fig. 5 which shows the relative difference $(Y_k^p - Y_k)/Y_k$ *vs.* Y_k, where Y_k and Y_k^p were obtained with points $(0, \phi_k)$ on the zero meridian with $\phi_k \geq 0$; as is observed such a difference is bounded by $\pm 2.5\%$ as Y_p goes from 0 to 1650 km. Nevertheless, the distance between (X_k, Y_k) and (X_k^p, Y_k^p) can be significant for the terrain height estimation as is seen below.

Figure 6 shows the difference $Y_k^p - Y_k$ *vs.* Y_k for the points $(0, \phi_k)$ of fig. 5 and we see that the difference increases monotonically from zero to several kilometers as Y_k goes

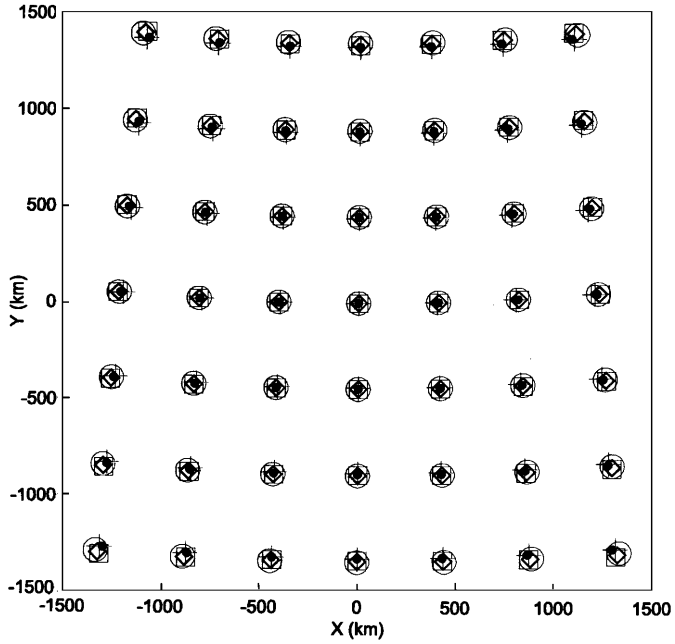

Fig. 4. – Points (X_k, Y_k) and (X_k^p, Y_k^p) on the region $\mathcal{D}_a$ of $\mathcal{T}$ corresponding to a data set $\{\lambda_k, \phi_k, h_k\}$ on the ellipsoid $\mathcal{E}$ WGS84 with height $h_k \equiv 0$. The tangency point P_c between $\mathcal{T}$ and $\mathcal{E}$ is at $\lambda_c = 0$ and $\phi_c = 24°$. The points (X_k, Y_k) obtained with the transformation T are denoted by $\bullet$, and the points (X_k^p, Y_k^p) obtained with the projections OSP, UTM, LP1 and LP2 are denoted by $\diamond$, $\square$, $\bigcirc$ and $+$, respectively.

from 0 to 1650 km (except for the LP2-projection). This implies that the true terrain elevation Z_k^p on (X_k^p, Y_k^p) *cannot* be computed on almost all points using the data λ_k, ϕ_k, h_k *alone* and, therefore, Z_k^p has to be estimated. A first approximation consists in estimating Z_k^p with the correct height Z_k on (X_k, Y_k),

$$Z_k^p \sim Z_k \,, \tag{3.6}$$

when (X_k^p, Y_k^p) is near (X_k, Y_k), of course. We can say that (X_k^p, Y_k^p) is near (X_k, Y_k) if it satifies the inequalities

$$|X_k^p - X_k| \le |\Delta X_k| \,, \qquad |Y_k^p - Y_k| \le |\Delta Y_k| \,, \tag{3.7}$$

where ΔX_k, ΔY_k denote the uncertainty of X_k, Y_k. Consider, for instance, the uncertainty $\Delta\lambda_k = \Delta\phi_k = 0$, $\Delta h_k = \pm 30$ m of some data from GTOPO30 [14], according to (2.16) we have $\Delta X_k \sim \pm 30$m and $\Delta Y_k \sim \pm 60$ m. For the points $(0, \phi_k)$ corresponding to figs. 5 and 6 we have $X_k^p = X_k = 0$ and (3.7) becomes $|Y_k^p - Y_k| \le 60$ m. Figure 7 shows the graph of $|Y_k^p - Y_k|$ *vs.* Y_k corresponding to the points $(0, \phi_k)$ of fig. 5, we observe that $|Y_k^p - Y_k| \le 60$ m holds with $Y_k^p \le Y_M^p$ where $Y_M^p \sim 5$, 195, 210, 245 km for the points (X_k^p, Y_k^p) from projections LP2, LP1, OSP and UTM, respectively. This means that (3.7) holds approximately for (X_k^p, Y_k^p) on the region

$$\mathcal{R}_a = [-250, 250] \times [-250, 250] \text{ km}^2 \,,$$

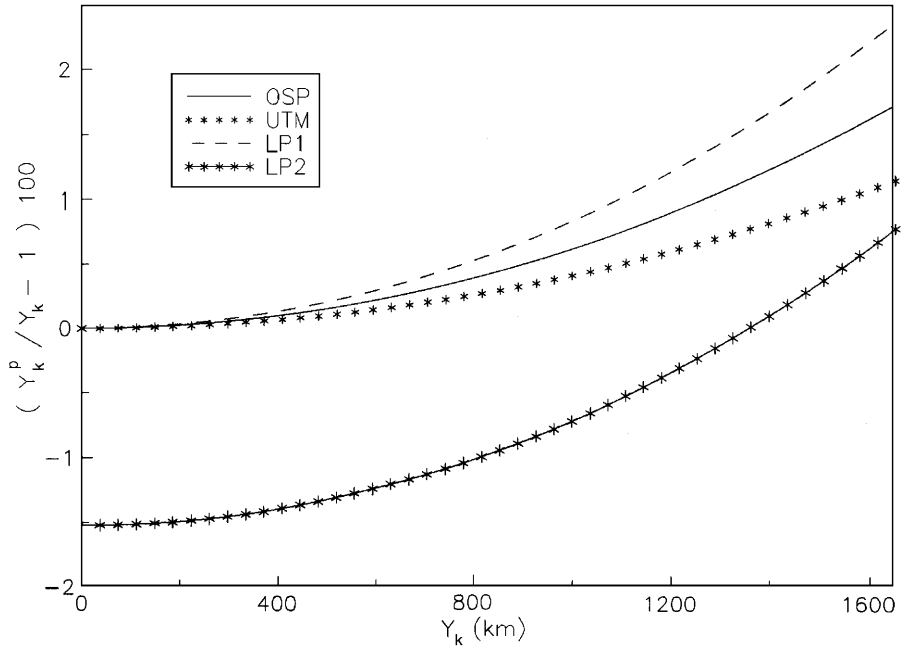

Fig. 5. – Graphs of $(Y_k^p/Y_k - 1)100$ *vs.* Y_k where Y_k^p and Y_k were obtained from points $(0, \phi_k)$ on the reference meridian of WGS84 $\mathcal{E}$ with $\phi_k \geq 0$. Y_k was computed with the transformation T and the Y_k^p's with the projection formulae given in the appendix.

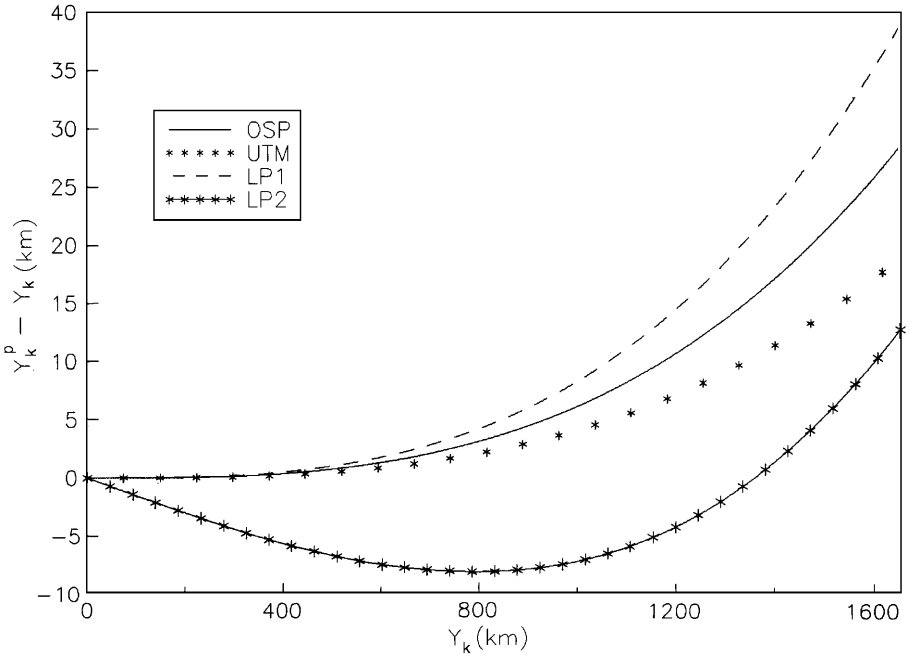

Fig. 6. – Graphs of $Y_k^p - Y_k$ *vs.* Y_k corresponding to the points $(0, \phi_k)$ of fig. 5.

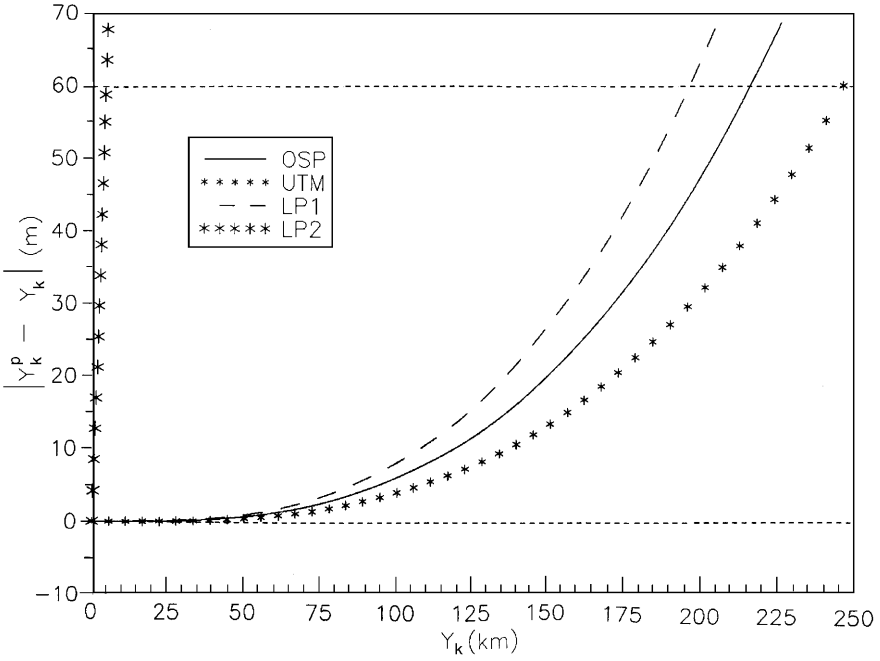

Fig. 7. – Graphs of $|Y_k^p - Y_k|$ *vs.* Y_k corresponding to the points $(0, \phi_k)$ of fig. 5.

when (X_k^p, Y_k^p) is obtained from projections LP1, OSP and UTM, while for (X_k^p, Y_k^p) from LP2, (3.7) is valid at most on the region

$$\mathcal{R}_b = [-10, 10] \times [-10, 10] \text{ km}^2.$$

Therefore, the approximation $Z_k^p \sim Z_k$ is valid if the points (X_k^p, Y_k^p) from projections OSP , UTM and LP1 (LP2) belong to $\mathcal{R}_a$ ($\mathcal{R}_b$). Of course, we have the approximation $Z_k^p \sim h_k$ but it is valid on a smaller region $\mathcal{R}_c$ as is shown below (eq. (3.10)). This points out a weakeness of map projections and, therefore, an error source in mesoscale modelation: If (X_k^p, Y_k^p) is far away from the boundary of $\mathcal{R}_a$ (as occurs with points on or near the boundary of $\mathcal{D}_a$, $\mathcal{D}_b$, $\mathcal{D}_c$) the true terrain elevation cannot be estimated reasonably with the sole data λ_k, ϕ_k, h_k and the estimations $Z_k^p \sim h_k$ and $Z_k^p \sim Z_k$ can yield a DEM on $\mathcal{T}$ with large terrain-height errors that deteriore the results of an atmospheric modelation. Furthermore, according to (2.16) if the data λ_k, ϕ_k, h_k were more accurate the regions $\mathcal{R}_a$ and $\mathcal{R}_b$ are smaller and, therefore, the application of map projections is less convenient to get a reliable DEM on domains such as $\mathcal{D}_a$, $\mathcal{D}_b$, $\mathcal{D}_c$. Finally, the relative smallness of regions $\mathcal{R}_a$ and $\mathcal{R}_b$ shows that the use of approximations $Z_k^p \sim h_k$ and $Z_k^p \sim Z_k$ cannot be justified by the sole visual appreciation of figs. 4 and 5.

3˙2. *Approximation* $Z_k^p \sim h_k$. – Since the correct height Z_k^p cannot be computed for almost all points (X_k^p, Y_k^p) we deal with the points (X_k, Y_k) for which the correct height Z_k can be estimated and used to study the correctness of the approximation

$$Z_k \sim h_k. \tag{3.8}$$

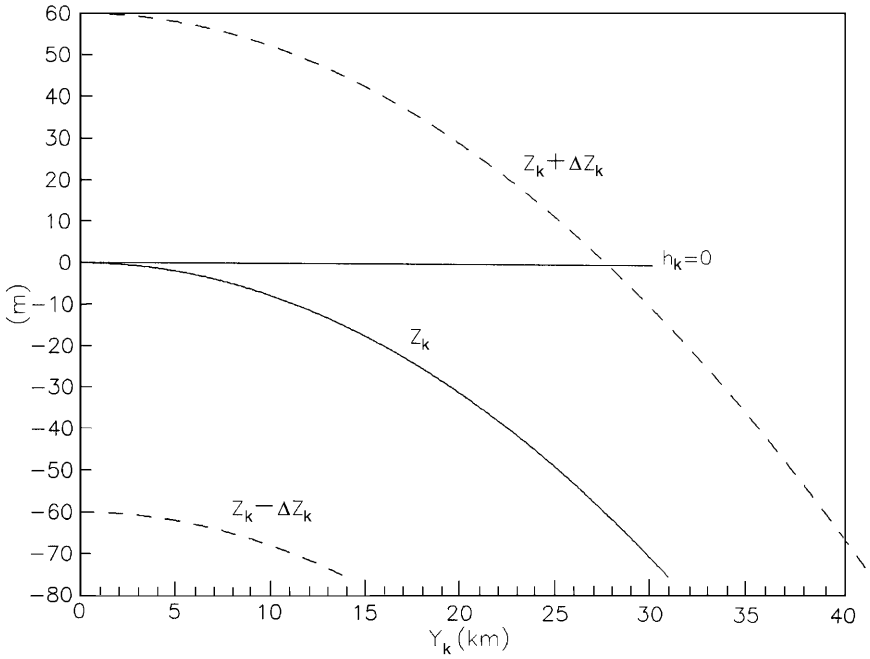

Fig. 8. – Graphs of Z_k, $Z_k \pm \Delta Z_k$, h_k *vs.* Y_k corresponding to the points $(0, \phi_k)$ of fig. 5.

We can say that (3.8) is valid if the approximating value h_k satisfies

$$|Z_k - h_k| \leq |\Delta Z_k|\,, \tag{3.9}$$

where the uncertainty ΔZ_k of Z_k can be estimated with $\Delta\lambda_k$, $\Delta\phi_k$, Δh_k (eq. (2.16)). Consider again $\Delta\lambda_k = \Delta\phi_k = 0$ and $\Delta h_k = \pm 30$ m, with $h_k \equiv 0$ and $\Delta Z_k \sim 60$ m (eq. (2.16)) the inequality (3.9) becomes $|Z_k - h_k| = |Z_k| \leq 60$ m. Figure 8 shows the graph of Z_k, $Z_k \pm \Delta Z_k$ and $h_k = 0$ *vs.* Y_k corresponding to the points $(0, \phi_k)$ of fig. 5, we see that $|Z_k| \leq 60$ m holds for Y_k in the interval $[0, 28$ km$]$ hence (3.8) is approximately valid on the region

$$\mathcal{R}_{\rm c} = [-30, 30] \times [-30, 30] \quad \text{km}^2. \tag{3.10}$$

This region is quite small with respect to $\mathcal{D}_a$, $\mathcal{D}_b$, $\mathcal{D}_c$ and $\mathcal{R}_a$ as well. Hence if Z_k^p is approximated by the corresponding datum h_k on $\mathcal{E}$, it is expected that such an approximating value has a large error when the approximation is applied on a whole domain such as $\mathcal{D}_a$, $\mathcal{D}_b$, $\mathcal{D}_c$. To get an idea of the error we plotted in fig. 9 the correct Z_k values *vs.* Y_k corresponding to the points $(0, \phi_k)$ of fig. 5. We see that the zero topography $h_k \equiv 0$ on $\mathcal{E}$ yields the correct height $Z(Y_{\max}) = -217, -61, -33$ and -5 km on the boundary point $(X = 0, Y_{\max})$ of regions $\mathcal{D}_a$, $\mathcal{D}_b$, $\mathcal{D}_c$ and $\mathcal{R}_a$, respectively. It is clear that there is no real height h_k on the Earth for which the approximation $Z(Y_{\max}) \sim h_k$ is valid at the boundary of $\mathcal{D}_a$, $\mathcal{D}_b$ and $\mathcal{D}_c$. If we consider that the usual height L_z of a tridimensional mesoscale domain is 20 km, the absolute error of the approximating value $h_k (\equiv 0)$ of Z_k is $|Z_k|$ or, equivalently, 1000%, 300% and 150% larger than 20 km on boundary of $\mathcal{D}_a$, $\mathcal{D}_b$,

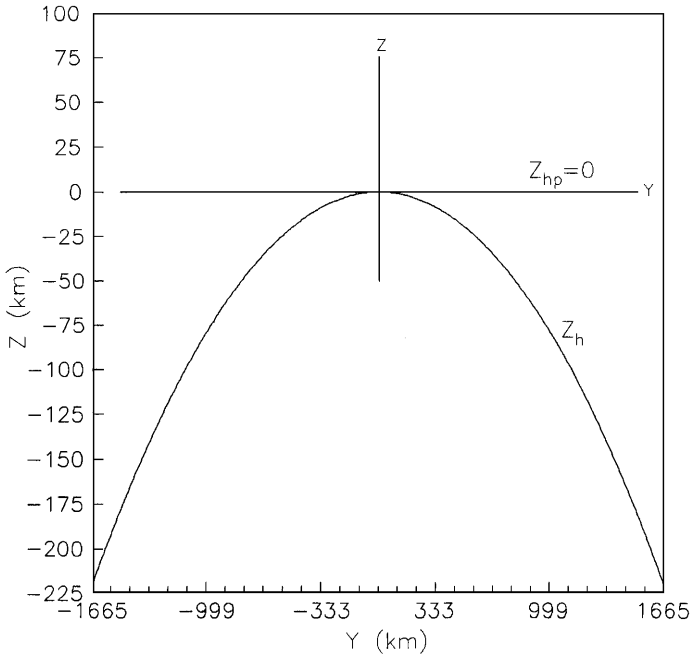

Fig. 9. – Graph of Z_k *vs.* Y_k corresponding to the points $(0, \phi_k)$ of fig. 5. The functions $Z_h(X, Y_k) = \sqrt{a^2 - Y_k^2} - a$ and $Z_{hp}(X, Y_k) = 0$ are plotted.

$\mathcal{D}_c$, respectively. This also shows that the procedure of taking a large horizontal model domain $\mathcal{D}$ to reduce the undesirable effects of lateral boundaries [1,3-5], can yield incorrect results if the DEM on $\mathcal{D}$ is obtained with map projections and the approximation $Z_k^p \sim h_k$.

4. – Mesoscale flow equations

In order to pose some meteorological problems generated by a topography defined via map projections in this section we carry out a comparison between mesoscale flow equations obtained from such a topography and those from a correct representation of topography. By simplicity the earth rotation is ignored and the flow is isothermic, incompressible and inviscid so that the model equations with respect to the XYZ system are

$$\nabla \cdot \vec{\mathbf{V}} = 0, \quad \frac{\mathrm{d}\vec{\mathbf{V}}}{\mathrm{d}t} + \frac{1}{\rho_0}\nabla P + g\hat{\mathbf{Z}} = 0\,,$$

where $\tilde{\mathbf{V}} = U\hat{\mathbf{X}} + V\hat{\mathbf{Y}} + W\hat{\mathbf{Z}}$ is the velocity vector, t is time, ρ_0 is the density, P is the air pressure and g the acceleration due to gravity, see, *e.g.*, [2, 4, 18].

To realistically represent topography mesoscale meteorological systems [1, 6-10] use a terrain-following coordinate system determined by the representation of topography in the XYZ system. The equations generated by the correct description of topography are obtained with the results of subsect. **2**˙2 as follows. If the topography equation

h =top(λ,ϕ) is known, eqs. (2.13*a*-*e*) yield the parametric equations of topography in the XYZ system

$$X = T_X[\lambda,\phi,\text{top}(\lambda,\phi)], \quad Y = T_Y[\lambda,\phi,\text{top}(\lambda,\phi)], \quad Z = T_Z[\lambda,\phi,\text{top}(\lambda,\phi)].$$

From the first two equations one obtains λ,ϕ in terms of X,Y and replacing these expressions in the third equation we get the topography equation

$$Z = Z_h(X,Y)\,, \tag{4.1}$$

which leads to the terrain-following coordinate system

$$y^1 = X, \quad y^2 = Y, \quad y^3 = H[Z - Z_h(X,Y)]/[H - Z_h(X,Y)], \tag{4.2}$$

where $H = \max Z$ is the height of the model domain. Model equations in the y^i system are written with the notation $X^1 = X$, $X^2 = Y$, $X^3 = Z$, $V^1 = U$, $V^2 = V$, $V^3 = W$, repeated indices in one term indicate summation, the transformation (4.2) and its inverse are denoted by $y^i(\vec{\mathbf{X}})$ and $X^j(\vec{\mathbf{y}})$, respectively. Thus the pressure and the (contravariant) components of velocity vector $\vec{\mathbf{v}}(\vec{\mathbf{y}})$ in the y^i system are

$$p(\vec{\mathbf{y}}) = P[X^j(\vec{\mathbf{y}})], \quad v^i(\vec{\mathbf{y}}) = V^j(\vec{\mathbf{X}})\partial y^i/\partial X^j. \tag{4.3}$$

The continuity and momentum equations are

$$\frac{1}{\sqrt{G}}\frac{\partial}{\partial y^i}\sqrt{G}v^i = 0, \quad \frac{\partial v^k}{\partial t} + v^m v^k{}_{,m} + G^{km}\frac{\partial p}{\partial y^m} + \delta_{3k}\frac{\partial y^k}{\partial X^3}g = 0\,, \tag{4.4}$$

where

$$v^k{}_{,m} = \Gamma^k_{ml}v^l + \frac{\partial v^k}{\partial y^m}, \quad \Gamma^k_{ml} = \frac{\partial^2 X^n}{\partial y^m \partial y^l}\frac{\partial y^k}{\partial X^n},$$

$\sqrt{G}$ is the Jacobian of transformation $y^i(\vec{\mathbf{X}})$ and G^{ki} is the inverse matrix of the metric tensor $G_{ij} = (\partial X^k/\partial y^i)(\partial X^k/\partial y^j)$.

Let us consider model equations from map projections. Map projection equations (3.1) together with h =top(λ,ϕ) and the approximation $Z^p_k \sim h_k$ yields the parametric equations of an approximate topography

$$X = P_X(\lambda,\phi), \quad Y = P_Y(\lambda,\phi), \quad Z = \text{top}(\lambda,\phi).$$

From the first two equations one gets expressions of λ, ϕ in terms of X, Y, which are replaced in top(λ,ϕ) to obtain a topographic equation

$$Z = Z_{hp}(X,Y)$$

which is an approximation of the correct equation $Z_h(X,Y)$. This leads to the terrain-following coordinate system:

$$y^1_p = X, \quad y^2_p = Y, \quad y^3_p = H[Z - Z_{hp}(X,Y)]/[H - Z_{hp}(X,Y)]. \tag{4.5}$$

Let $y_p^i(\vec{\mathbf{X}})$ and $X^j(\vec{\mathbf{y}}_p)$ denote the transformation (4.5) and its inverse. Thus the pressure and components of the velocity vector $\vec{\mathbf{v}}_p(\vec{\mathbf{y}}_p)$ in the y_p^i system are

$$p_p(\vec{\mathbf{y}}_p) = P[X^j(\vec{\mathbf{y}}_p)], \quad v_p^i(\vec{\mathbf{y}}_p) = V^j(\vec{\mathbf{X}})\partial y_p^i/\partial X^j.$$

The continuity and momentum equations are

$$\frac{1}{\sqrt{G_p}}\frac{\partial}{\partial y_p^i}\sqrt{G_p}v_p^i = 0, \quad \frac{\partial v_p^k}{\partial t} + v_p^m v_{p,m}^k + G_p^{km}\frac{\partial p_p}{\partial y_p^m} + \delta_{3k}\frac{\partial y_p^k}{\partial X^3}g = 0\,, \tag{4.6}$$

where the index p denotes quantities in the y_p^i system.

Mesoscale models that use map projections to define topography in the XYZ system solve equations like (4.6) which are approximations of eqs. (4.4) generated by the correct topography equation $Z_h(X,Y)$. The results of sect. **3** show that the error of $Z_{hp}(X,Y)$ can be larger than the height H used in some mesoscale studies, a result that can invalidate the usefulness of model equations like (4.6). In principle we have to solve eqs. (4.4) and (4.6) with pertinent boundary conditions to compare the meteorological fields and determine the error generated by the innacuracy of $Z_{hp}(X,Y)$, this is not an easy task because there are no analytical solutions for problems with complex topography. To get precise meteorological fields we consider the stationary flow around a two-dimensional earth with radius a and topography $\mathrm{top}(\lambda,\phi) = 0$ as fig. 9 shows, so that the governing equations are

$$\nabla\cdot\vec{\mathbf{V}} = 0, \quad \frac{1}{\rho_0}\nabla P = -(\vec{\mathbf{V}}\cdot\nabla)\vec{\mathbf{V}} - g\hat{\mathbf{Z}}. \tag{4.7}$$

The topography equation and the boundary condition for $\vec{\mathbf{V}}$ are

$$Z_h(X,Y) = -a + \sqrt{a^2 - Y^2}, \quad \vec{\mathbf{V}}\cdot\hat{\mathbf{n}}|_{Z=Z_h} = 0. \tag{4.8}$$

The velocity $\vec{\mathbf{V}}$ that satisfies the boundary condition and the continuity equation can be obtained from the flow around a circular cylinder and is

$$V = V_0(1 + R^{-2} - 2\bar{y}^2R^{-4}), \quad W = -2V_0\bar{y}(1+\bar{z})R^{-4}\,, \tag{4.9}$$

where $R = [\bar{y}^2 + (1+\bar{z})^2]^{1/2}$, $\bar{y} = Y/a$, $\bar{z} = Z/a$. The pressure P is obtained from the momentum equation. The pressure $p(\vec{\mathbf{y}})$ and velocity $\vec{\mathbf{v}}(\vec{\mathbf{y}})$ in terrain-following coordinates y^i are obtained from (4.3) but to analyse the fields $p_p(\vec{\mathbf{y}}_p)$, $\vec{\mathbf{v}}_p(\vec{\mathbf{y}}_p)$ from map projections it is enough to work with P and $\vec{\mathbf{V}}$. From (4.5) it follows that the equation $\mathrm{top}(\lambda,\phi) = 0$ yields $Z_{hp}(X,Y) = 0$ and the terrain-following coordinates

$$y_p^1 = X, \quad y_p^2 = Y, \quad y_p^3 = Z$$

for *any* map projection, hence the governing equations are

$$\nabla\cdot\vec{\mathbf{v}}_p = 0, \quad \frac{1}{\rho_0}\nabla p_p = -(\vec{\mathbf{v}}_p\cdot\nabla)\vec{\mathbf{v}}_p - g\hat{\mathbf{Z}}\,,$$

TABLE I. – *Terrain elevation Z_h (eq. (4.8)), components $V(Y,Z)$, $W(Y,Z)$ (eq. (4.9)), $v_p(Y,Z)$, $w_p(Y,Z)$ (eq. (4.10)), and percentage error δv_p for some Y values with $a = 6378$ km and $V_0 = 5$ ms^{-1}.*

Y	Z_h	$V^{(a)}$	$W^{(a)}$	$\delta v_p^{(a)}$	$V^{(b)}$	$W^{(b)}$	$\delta v_p^{(b)}$
0	0.0	10.0	.00	0.0	10.0	.00	0.0
250	−4.9	10.0	−.39	0.2	10.0	−.39	0.2
650	−19.6	9.8	−1.00	1.6	9.9	−1.01	1.1
882	−78.9	9.7	−1.33	2.9	9.8	−1.37	1.9
1665	−178.9	9.1	−2.29	10.1	9.3	−2.52	7.3
		v_p	w_p		v_p	w_p	
		10.0	0.0		10.0	0.0	

(*a*) Calculations with $Z = 0$.
(*b*) Calculations with $Z = \sqrt{a^2 - Y^2} - a$.

with the boundary condition $v_p^3(X, Y, Z = 0) = 0$. The solution to this problem is a uniform flow and if the condition $\vec{\mathbf{V}} = \vec{\mathbf{v}}_p$ is imposed on $Y = Z = 0$, eq. (4.9) yields

$$\vec{\mathbf{v}}_p = v_p \hat{\mathbf{Y}} + w_p \hat{\mathbf{Z}} \quad \text{with } v_p = 2V_0, \quad w_p = 0, \tag{4.10}$$

$p_p(\vec{\mathbf{y}}_p)$ is easily obtained. The pressure $P(Y,Z)$ is usually calculated from the momentum equation by solving $\rho_0^{-1}\nabla^2 P = -\nabla\cdot[(\vec{\mathbf{V}}\cdot\nabla)\vec{\mathbf{V}}]$ but to simplify computations we compare the isobars which are calculated as follows. Let $Z^*(Y; Y_0, Z_0)$ and $Z_p^*(Y; Y_0, Z_0)$ be the isobars that pass by (Y_0, Z_0),

$$P[Y, Z^*(Y; Y_0, Z_0)] = P[Y_0, Z_0], \quad p_p[Y, Z_p^*(Y; Y_0, Z_0)] = p_p[Y_0, Z_0].$$

If we impose the boundary condition

$$P(Y_0 = 0, Z_0) = p_p(Y_0 = 0, Z_0)$$

$P(Y,Z)$ and $p_p(Y,Z)$ have the same pressure value on the isobars $Z^*(Y; 0, Z_0)$ and $Z_p^*(Y; 0, Z_0)$, respectively. We have $Z_p^*(Y; 0, Z_0) = Z_0$ and Z^* is obtained by solving the ordinary differential equation

$$\frac{\partial P}{\partial Y} + \frac{\partial P}{\partial Z}\frac{\mathrm{d}Z^*}{\mathrm{d}Y} = 0 \quad \text{with } Z^*(0; 0, Z_0) = Z_0.$$

From eqs. (4.7) and (4.9) we get the equation

$$\frac{\mathrm{d}Z^*}{\mathrm{d}Y} = -\frac{Wa^{-1}\{V(1+\bar{z})^{-1}[-3 + 4\bar{y}^2/R^2] + W\bar{y}^{-1}[1 + 4\bar{y}^2/R^2]\}}{Wa^{-1}\{V\bar{y}^{-1}[-1 + 4\bar{y}^2/R^2] + W(1+\bar{z})^{-1}[1 + 4(1+\bar{z})^{-2}/R^2]\} - g}$$

which is solved numerically by the Gear method.

Table I reports the correct terrain elevation $Z_h(X,Y)$, velocity components V, W and the percentage error $\delta v_p = |v_p/V - 1| \times 100$ for $Z = 0$, $\sqrt{a^2 - Y^2} - a$, $Y \in$[0,1665 km], $a = 6378$ km and $V_0 = 5$ ms^{-1}, with $v_p = 2V_0$ and $w_p = 0$ for all Y, Z. Table II reports

TABLE II. – *Points* $(Y, Z^*(Y;0,0))$ *and* $(Y, Z_p^*(Y;0,0))$ *on the isobars* $P(Y,Z^*) = P(0,0)$ *and* $p_p(Y,Z_p^*) = p_p(0,0)$. *Notation* $1.6[-5]$ *means* 1.6×10^{-5}.

Y	0	250	650	882	1665
Z^*	0	1.6[−5]	1.0[−4]	1.9[−4]	6.3[−4]
Z_p^*	0	0	0	0	0

some points (Y, Z^*) and (Y, Z_p^*) of the isobars that pass by $Y_0 = Z_0 = 0$. We observe that δv_p increases from 0 to 10% as Y goes from 0 to 1665 km while $|Z_h|$ and $|W|$ increase up to 179 km and 2.52 ms^{-1}, respectively, although the isobars $Z^*(Y;0,0)$ and $Z_p^*(Y;0,0)$ are essentially the same. The difference between $\vec{\mathbf{V}}$ and $\vec{\mathbf{v}}_p$ is large for $Y \in$[0,1665] and it is clear that such a difference comes from the innacuracy of $Z_{hp}(X,Y)$, which in turn is generated by the "earth curvature" and the use of map projections. Of course, in this example we have ignored important factors controling the fluid motion such as the tridimensional nature of the problem, the earth rotation, the stratification, a complex topography and the time evolution of atmospheric flows, but we may expect that these factors will generate larger differences between the meteorological fields obtained from the correct topography $Z_h(X,Y)$ and those from $Z_{hp}(X,Y)$. To this we have to add the known fact that in a *nonstationary* flow the differences between velocities $\vec{\mathbf{V}}$, $\vec{\mathbf{v}}_p$ and pressures P, p_p reported in tables I, II can generate qualitatively different mesoscale flows as the time t increases because of the nonlinearity of governing equations [19]. These differences may be particularly important for some mesoscale meteorological applications such as the study of diffusion and transport of pollutants which are phenomena that depend of an accurate description of small-scale motions [20, 21].

5. – Conclusions

The atmospheric modelation is benefited by the international effort to develop accurate Digital Elevation Models $\{\lambda_k, \phi_k, h_k\}$ with respect to an ellipsoidal Earth model $\mathcal{E}$ because, in principle, the effects of topography can be considered with some detail. The transformation T provides a simple way to take advantage of such an effort because it yields a DEM $\{X_k, Y_k, Z_k\}$ on the tangent plane $\mathcal{T}$ of interest, as good as the original one. In fact, we showed that i) T yields the unique points (X_k, Y_k) on $\mathcal{T}$ (module a unit of length) for which we can compute the correct terrain elevation Z_k using the data λ_k, ϕ_k, h_k alone, and ii) the uncertainty in X_k, Y_k, Z_k is bounded linearly by the one of λ_k, ϕ_k, h_k.

Map projections were developed with the purpose of transfering places on an Earth model $\mathcal{E}$ to points on a flat sheet of paper. This poses the nontrivial problem of estimating the correct terrain elevation when map projections are used to get a DEM with respect to a tangent plane $\mathcal{T}$ because map projections yield points (X_k^p, Y_k^p) on $\mathcal{T}$ without considering the terrain height information. In fact, since the distance between a point (X_k^p, Y_k^p) and the point (X_k, Y_k) for which we know the correct height Z_k increases from zero to several kilometers as (X_k^p, Y_k^p) moves away from the origin $(0,0)$ (see fig. 6), the height Z_k^p on (X_k^p, Y_k^p) cannot be calculated correctly using the corresponding data λ_k, ϕ_k, h_k alone. The use of the uncertainty reported for data from GTOPO30, showed that the approximations $Z_k^p \sim h_k$ and $Z_k^p \sim Z_k$ are valid or consistent with the accuracy of

the data λ_k, ϕ_k, h_k on a region $\mathcal{R}$ that may be small with respect to a model domain such as $\mathcal{D}_a$, $\mathcal{D}_b$, $\mathcal{D}_c$. Consequently the application of such approximations beyond $\mathcal{R}$ can yield a terrain height whose absolute error is similar or larger than the height of a tridimensional mesoscale domain (fig. 9). The estimation of $\mathcal{R}$ is possible only with the knowledge of $\Delta\lambda_k$, $\Delta\phi_k$, Δh_k, if it were unknown (as occurs with some data bases including GTOPO30) the use of map projections to get a DEM on domains such as $\mathcal{D}_a$, $\mathcal{D}_b$, $\mathcal{D}_c$, may have no sense because of the uncertainty of the estimated DEM. Probably, map projections do not correspond with the international tendency to develop both accurate DEMs and mesoscale models that consider with more detail the topography. As the data become more accurate the region of correctness of approximations $Z_k^p \sim h_k$ and $Z_k^p \sim Z_k$ becomes smaller and hence sophisticated methods have to be used in order to get a DEM on the points (X_k^p, Y_k^p) with an accuracy that is consistent with that of the original DEM. Instead of this it may be more easy to use the DEM given by the transformation T.

Throughout the manuscript we have considered how to get a reliable DEM on a tangent plane $\mathcal{T}$ with a given DEM on a ellipsoidal Earth model $\mathcal{E}$, but this does not solve the problem of getting a DEM with the horizontal resolution of a given computational grid. Several methods have been proposed in the literature (see, *e.g.*, [8,9]) and it is clear that we can use them with the DEM given by the transformation T instead of the DEM obtained via map projections.

The fact that the Earth curvature generates a terrain height as $Z_k = -217, -60$ or -33 km for regions $\mathcal{D}_a$, $\mathcal{D}_b$, $\mathcal{D}_c$ suggests that such a horizontal domain may not be the best choice to consider topographic effects on the atmosphere on a model domain as large as them. For instance, to describe correctly the topography on $\mathcal{D}_b$ we have to use a tridimensional model region with a height of approximately 75 km instead of 17.8 km used in ref. [16] increasing the computational cost of the mesoscale modelation. Probably, the effects of the Earth curvature become important or are better represented in a tridimensional region that uses a spherical horizontal domain such as that described in subsect. **2**˙3.

There has been an increasing need to assess the uncertainty in mesoscale meteorological models (MMMs) as input to air quality models; for instance, if the wind field is wrong no level of sophistication in the atmospheric chemistry will remedy the error due to this deficiency. It is known that MMMs have an uncertainty that arises from factors such as the spatial resolution, the uncertainty in the initial meteorological fields or the kind of turbulence models and the results of this work suggest that the innacuracy of a topography obtained via map projections may be an important source of uncertainty. Apparently there is no physical, mathematical or computational motivation to use this kind of topographic models, instead of them one may employ the DEMs obtained with the results of sect. **2**. Up to date many studies have used MMMs with a map-projection topography and the complexity of model equations makes too difficult the estimation of the error generated by such topographic models. It seems that the best way to determine this error is to carry out calculations with the DEMs obtained with the transformations of sect. **2** and compare results.

* * *

The author wish to thanks Prof. R. Maria Velasco by the revision of the manuscript, and H. Hernández and D. Romero by their support.

Appendix A.

Projection formulae

The formuale for $\mathcal{E}$ with $\epsilon = 0$ and $R = a$ were taken from [12, 13] and modified to satisfy (3.2) with $\lambda_0 = \lambda_c = 0$ and $\phi_0 = \phi_c = 24°$. Oblique stereographic projection ([13], p. 63)

$$\begin{aligned} X^p &= 2R\zeta^{-1}\cos\phi\sin\lambda\,, \\ Y^p &= 2R\zeta^{-1}(\cos\phi_c\sin\phi - \sin\phi_c\cos\phi\cos\lambda)\,, \end{aligned}$$

with $\zeta = 1+\sin\phi_c\sin\phi+\cos\phi_c\cos\phi\cos\lambda$. Universal transverse mercator projection [12]

$$\begin{aligned} X^p &= 2^{-1}R\log[(1+\cos\phi\sin\lambda)/(1-\cos\phi\sin\lambda)]\,, \\ Y^p &= R\tan^{-1}[\tan\phi/\cos\lambda] - R\phi_c\,. \end{aligned}$$

Lambert projection [12] with one standard parallel at ϕ_c: we set $\rho_c = R\cot\phi_c$ and $\rho(\phi) = [\tan(\pi/4-\phi/2)/\tan(\pi/4-\phi_c/2)]^{\sin\phi_c}$ to obtain [12]

$$X^p = \rho_c\rho(\phi)\sin(\lambda\sin\phi_c), \quad Y^p = \rho_c[1-\rho(\phi)\cos(\lambda\sin\phi_c)].$$

Lambert projection [12] with two standard parallels at ϕ_1 and ϕ_2 ($\phi_1 < \phi_2$): we define $\rho_1 = R\cos\phi_1/\sin\phi_0$ with [12]

$$\sin\phi_0 = \frac{\log[\cos\phi_1/\cos\phi_2]}{\log[\tan(\pi/4-\phi_1/2)/\tan(\pi/4-\phi_2/2)]}$$

and $\rho_2(\phi) = \rho_1[\tan(\pi/4-\phi/2)/\tan(\pi/4-\phi_1/2)]^{\sin\phi_0}$ to get

$$X^p = \rho_2(\phi)\sin(\lambda\sin\phi_0), \quad Y^p = \rho_2(\phi_c) - \rho_2(\phi)\cos(\lambda\sin\phi_0).$$

REFERENCES

[1] Pielke R. A., *The Status of Mesoscale Meteorological Models.* In *Planning and Managing Regional Air Quality*, edited by P. A. Solomon and T. A. Silver (Pacific Gas & Electric Co. and Lewis Publishers, San Ramon, CA) 1994, pp. 435-463.

[2] Hooijberg M., *Practical Geodesy Using Computers* (Springer, Berlin) 1997.

[3] Pielke R. A., *Mesoscale Meteorological Modeling* (Academic Press, New York) 1984.

[4] Perkey D. J., *Formulation of Mesoscale Numerical Models.* In *Mesoscale Meteorology and Forecasting*, edited by P. S. Ray (American Meteorological Society, Boston) 1986, pp. 578-579.

[5] Eppel D. P. and Callies U., *Boundary Conditions and Treatment of Topography in Limited-Area Models*, in *Diffusion and Transport of Pollutants in Atmospheric Mesoscale Flow Fields*, edited by A. Gyr and F.-S. Rys (Kluwer, Netherlands) 1995.

[6] Pielke R. A. and Coauthors, *Meteorol. Atmos. Phys.*, **49** (1992) 69, `http://www.aster.com/aster/docs/rams_techman.pdf`, sections 2.2 and 10.7.

[7] Grell G. A., Dudhia J. and Stauffer D. R., *A Description of the Fifth-Generation Penn State/NCAR Mesoscale Model (MM5)* chap. 4, NCAR Technical Note, NCAR/TN-398+STR (1994).

[8] Guo Y.-R. and Chen S., *Terrain and Land Use for the Fifth-Generation Penn State/NCAR Mesoscale Modeling System (MM5): Program Terrain*, NCAR Technical Note, NCAR/TN-397+IA, 1994, `http://box.mmm.ucar.edu/mm5/documents/`.
[9] Xue M., Droegemeler K. K., Wong V. and Brewster K., *Advanced Regional Prediction System (ARPS) Version 4.0 User's Guide*, 1995, chaps. 7 and 8, `http://wwwcaps.ou.edu/ARPS/`.
[10] Brown J. M. and Williams M., *HOTMAC Input Guide*, chap. 2. Internal Report, LA-UR-98-1365, Los Alamos National Laboratory, 1998, `http://www-tsa.lanl.gov/tsa4/pdf/air/hotmac.input.pdf`.
[11] Haltiner G. J., *Numerical Weather Prediction* (Wiley and Sons, New York) 1971, pp. 13-18.
[12] Pearson F., *Map Projections: Theory and Applications* (CRC Press, Boca Raton FL) 1990.
[13] Richardus P. and Adler R. K., *Map Projections for Geodesists, Cartographers and Geographers* (North-Holland, Amsterdam) 1972.
[14] GTOPO30 documentation, section 7, U.S. Geological Survey (1997). `http://www.scd.ucar.edu/dss/datasets/ds758.0.hmtl`.
[15] *Pronóstico Numerico Regional (Modelo MM5)*, Servicio Meteorólogico Nacional and Instituto Mexicano de Tecnologia del Agua, `http://galileo.imta.mx/mm5/`.
[16] Fast J. D. and Zhong S., *J. Geophys. Res.*, **103** (1998) 18927.
[17] Yamada T., Kao J. C.-Y. and Bunker S., *Atmos. Environ.*, **23** (1989) 539.
[18] Atkinson W. B., *Introduction to the fluid mechanics of meso-scale flow fields*, in *Diffusion and Transport of Pollutants in Atmospheric Mesoscale Flow Fields*, edited by A. Gyr and F.-S. Rys (Kluwer, Netherlands) 1995.
[19] Monin A. S. and Piterbarg L. I., *Forecasting weather and climate*, in *Limits of Predictability*, edited by Y. Kravtov (Springer, Berlin) 1993.
[20] Pielke R. A., *Atmos. Environ.*, **32** (1998) 1467.
[21] Pielke R. A. and Uliaz M., *Atmos. Environ.*, **32** (1998) 1455.